

Interstellar extinction in Orion. Variation of the strength of the UV bump across the complex.

Leire Beitia-Antero,¹[★] Ana I. Gómez de Castro,¹[†]

¹*AEGORA Research Group, Universidad Complutense de Madrid, Facultad de CC. Matemáticas, Plaza de Ciencias 3, E-28040 Madrid*

Accepted XXX. Received YYY; in original form ZZZ

ABSTRACT

There is growing observational evidence of dust coagulation in the dense filaments within molecular clouds. Infrared observations show that the dust grains size distribution gets shallower and the relative fraction of small to large dust grains decreases as the local density increases. Ultraviolet (UV) observations show that the strength of the 2175 Å feature, the so-called UV bump, also decreases with cloud density. In this work, we apply the technique developed for the Taurus study to the Orion molecular cloud and confirm that the UV bump decreases over the densest cores of the cloud as well as in the heavily UV irradiated λ Orionis shell. The study has been extended to the Rosette cloud with uncertain results given the distance (1.3 kpc).

Key words: ISM: dust, extinction

1 INTRODUCTION

The Interstellar Medium (ISM) is a complex ensemble of gas, large molecules and dust coupled through the action of the magnetic fields permeating the Galaxy. In some parts of the Galaxy, molecular clouds are formed due to galactic stresses (Elmegreen (1990); Franco et al. (2002)) or eventual accretion from the intergalactic medium (Mirabel (1982); Wang et al. (2004)). In the outskirts of these clouds the dust size distribution varies due to density gradients that determine the characteristics of the stars that will be formed inside them (see e.g. Dzyurkevich et al. (2017)). Particularly, small dust grains are relevant because they act as main carriers of the field and set the fundamental scales for ambipolar diffusion and magnetic waves propagation (Pilipp et al. (1987)), favouring the coupling of the cloud with the ambient field up to cut-off wavelengths of 0.1pc (Nakano (1998)).

The distribution of large dust grains has been studied, for instance, by The Herschel Space Telescope. It has provided measurements of this population in the nearest molecular complexes such as Taurus (Ysard et al. (2013)) and Orion (Roy et al. (2013); Stutz & Kainulainen (2015)). On the other hand, the most sensitive way to detect variations in the distribution of small dust grains (<0.05 microns) and large molecules (such as the Polycyclic Aromatic Hydrocarbons or PAHs) is to measure the strength of the 2175 Å

feature of the extinction curve, the so-called UV bump. The UV bump is, by far, the strongest spectral feature in the extinction curve but its source remains uncertain (see e.g. the review by Draine (2003)). Though small graphite grains were proposed initially as the main source of the bump, the baseline today are PAHs (Weingartner & Draine (2001)), that share with a graphite sheet a similar structure in terms of the distribution of the carbon atoms. PAHs are required to reproduce the observed infrared emission (Leger & Puget (1984)) and they somewhat represent the extension of the dust grain size distribution into the molecular domain.

The relative fraction of the smallest components of dust grains in the ISM can be modified through coagulation into larger particles in regions of high density or through destruction by a strong ultraviolet radiation field. In a previous work, we developed a method to explore the former process applying the star counts method in the near ultraviolet (NUV) (Gómez de Castro et al. (2015), hereafter GdC2015), using the *All Sky Survey* (AIS) carried out by the Galaxy Evolution Explorer (GALEX) The method was successfully applied to the Taurus molecular complex and we found evidence of a decreasing UV bump strength as approaching to the densest parts of the clouds, in excellent agreement with Spitzer-based results (Flagey et al. (2009)).

In this work, we apply the same method to the Orion molecular cloud to detect possible dust coagulation processes and to explore the impact of the strong UV background in the PAHs survival. Orion spans more than 700deg² in the sky and it contains three main molecular structures: the Orion

[★] E-mail: lbeitia@ucm.es

[†] E-mail: aig@ucm.es

A ($d = 371 \pm 10pc$) and Orion B ($d = 398 \pm 12pc$) clouds and the λ Orionis ring ($d = 445 \pm 50pc$) (distances from Lombardi et al. (2011)). In Section 2, the method is shortly described and in Sections 3 and 4, it is applied to the Orion star forming region. Evidence of UV bump suppression close to the dense filaments is found, as well as deviations from the ISM law around the heavily irradiated area of λ Orionis. Finally, in Section 5, the work has been extended to the nearby (in projection) Rosette cloud. Ultraviolet spectroscopic observations are available for some Rosette stars that have been used to test the statistical quality of the results. A brief summary is provided in Section 6.

2 METHOD DESCRIPTION

The method is based on the extensively used extinction model derived by Fitzpatrick & Massa (2007) (hereafter FM07). GdC2015 show that the strength of the bump can be expressed in terms of extinction in the GALEX NUV band, A_{NUV} , and in the K infrared band, A_{K} , as,

$$A_{\text{bump}} = (0.106 \pm 0.008) \frac{A_{\text{NUV}}}{A_{\text{K}}} + (2.0 \pm 0.3) \quad (1)$$

where A_{bump} is the strength of the bump in the extinction curve (FM07). This result simply indicates that the ISM extinction law admits a fairly simple parametric approximation from the near infrared to near ultraviolet except for the strength of the bump.

A_{K} has been evaluated for the nearby molecular clouds by Froebrich et al. (2007) (hereafter F07) based on data from the 2MASS survey (Skrutskie et al. (2006)). A_{NUV} may be calculated by using the star counts method (GdC2015) that has been extensively used in astronomy (Bok & Cordwell (1973)). For example, this method was applied by Lombardi et al. (2011) to estimate the distances to the main components of the Orion complex ($d(\text{Ori A}) = 371 \pm 10pc$, $d(\text{Ori B}) = 398 \pm 12pc$, $d(\lambda \text{ Ori}) = 445 \pm 50pc$).

In its most usual application, star counts in a given field are compared with the predictions for an unextinguished, nearby field and the extinction is given by,

$$A_{\text{NUV}} = \frac{1}{b_{\text{NUV}}} \log(N_{\text{NUV}}^*/N_{\text{NUV}}) \quad (2)$$

where N_{NUV} are the observed counts, N_{NUV}^* are the expected counts from a non-extinguished field, and $b_{\text{NUV}} = d \log N(m_{\text{NUV}})/dm_{\text{NUV}}$ (with m_{NUV} , the apparent magnitude at wavelength NUV) is a measure of the slope of the luminosity function in the area under study. As the NUV luminosity function has not been determined for the Galaxy yet, we have derived it for the Orion region using GALEX data.

The resolution of the maps created by these means depends on the angular size of the region used to measure the star counts that becomes the picture element, the pixel, of the extinction map. A compromise must be sought between resolution and good statistics. Large pixel sizes are ideal for deducing statistical properties but, in practice, averaging the extinction over a large area smooths the results. Small pixel sizes provide a cleaner idea of the distribution of the obscuring material but the statistics may become very poor and, with them, the extinction measurements. Based on our previous experience (GdC2015), we have worked with three

pixel sizes: 30arcmin, 15arcmin and 10arcmin (see Section 4 for a discussion of the results).

3 DATA PROCESSING

3.1 Data

The GALEX mission was intended to survey the ultraviolet sky avoiding the Galactic Plane, as well as regions with bright sources that could damage the detectors (Martin et al. (2005)). GALEX images (or tiles) were obtained in two UV bands: Far Ultraviolet (FUV) band and Near Ultraviolet (NUV) band, with a circular field of view of 1.2° . The GALEX AIS was completed in 2007 and covers $\sim 26,000\text{deg}^2$. Point-like sources were extracted from the images to generate the GALEX catalogue (Bianchi et al. (2012)) that is used as a baseline for this work; only NUV data will be used due to statistical reasons since GALEX detected ~ 10 times more sources in NUV band than in FUV band.

In the Orion region, the survey consists of 359 images (or tiles): $\sim 406\text{deg}^2$, including a small fraction of the Orion A cloud and part of the λ Orionis ring. To remove spurious sources, the NUV sources in the catalogue were cross-correlated with the 2MASS catalogue (see Gómez de Castro et al. (2011); Bianchi et al. (2011) for details). Only NUV sources with 2MASS counterpart in a search radius of 3arcmin were considered bona-fide sources for the application of the star counts method (Gómez de Castro et al. (2015)). The selection of the NUV sources in the Orion region was obtained in the same manner (Sánchez et al. (2014), hereafter S2014); the final sample amounts to a total of 289,968 NUV sources. Their spatial distribution is shown in Figure 1 together with F07's A_{V} -map as a reference. Also overplotted are the 111 Young Stellar Objects candidates determined by S2014; concentrations are observed towards the Orion A cloud and the λ Orionis ring.

The sensitivity of the star counts method depends on the vast majority of the stars being background to the cloud under study. As the Orion cloud is at ~ 400 pc from the Sun, most sources are expected to be background. The release of the Gaia DR1 catalogue (Gaia Collaboration et al. (2016)) has allowed an assessment of the fraction of foreground stars. Unfortunately, only 13,562 stars have been found in the GAIA - GALEX cross-match; *i.e.* about 4.7% of the sample. 33% of these sources (4,444) are foreground stars; this factor is an upper limit since GAIA's first release is not complete neither in brightness (it is balanced to nearby sources) nor in direction (Gaia Collaboration et al. (2016)). Note that the contribution of foreground sources can be neglected if they are uniformly distributed over the field and the density of foreground sources is much smaller than the density of background sources¹, which is the case.

¹ Let be N_0 the density of foreground sources, then Eq. 2 changes to $A_{\text{NUV}} = \frac{1}{b_{\text{NUV}}} \log\left(\frac{N_{\text{NUV}}^* + N_0}{N_{\text{NUV}} + N_0}\right)$ and, $A_{\text{NUV}} = \frac{1}{b_{\text{NUV}}} \log\left(\frac{1 + N_{\text{NUV}}^*/N_0}{1 + N_{\text{NUV}}/N_0}\right)$.

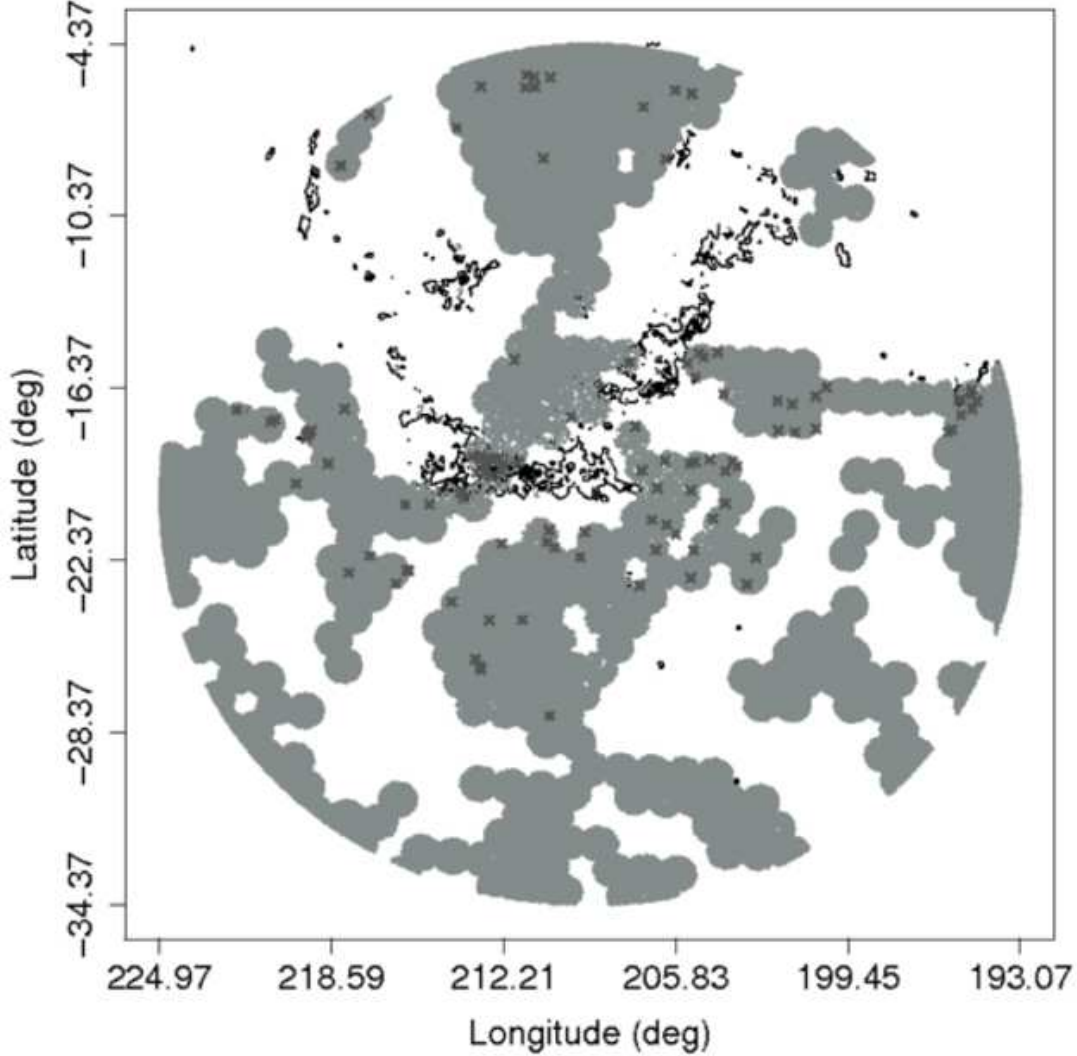


Figure 1. Distribution of the GALEX NUV sources centered in Orion in a search radius of $r = 15^\circ$ superimposed on the infrared dust map by F07. Note that the 0.6° radius field of the GALEX tiles is clearly recognisable. Marked with a cross are the Young Stellar Object candidates from S2014.

3.2 Calculation of the A_{NUV} map

In order to evaluate the map it is necessary to determine the slope of the NUV luminosity function in Orion and to select the reference field for the calculation of the extinction. As the area mapped is 406° wide, and extends over about 30° in galactic latitude and longitude, some precautions need to be taken. Firstly, possible deviations of the luminosity function across the region must be evaluated. Then, as the density of stars decreases with galactic latitude, it is required to correct for this effect when defining the N_{NUV}^* for each galactic latitude.

3.2.1 NUV Luminosity function

The region was divided in square regions of $2^\circ \times 2^\circ$ over which we computed the luminosity function; among them we chose ten, apparently non-extinguished comparing to IRIS and Planck dust maps. In each case, we fitted the slope of the luminosity function in the 16-20 mag interval (the completeness region) by ordinary least squares obtaining the values in Table 1.

Then we tested whether there were significant variations with galactic latitude or longitude and not finding such a trend, we computed a weighted mean obtaining $b_{\text{NUV}} = 0.276 \pm 0.004$, which is quite similar to but smaller than the value obtained in Taurus ($b_{\text{NUV}} = 0.294 \pm 0.002$, GdC2015).

Table 1. Least-squares fitting results of the NUV luminosity function for the 10 regions in Orion in the 16-20mag interval. $*S_r$: residual standard error.

Region	Stars	b_{NUV}	$e_{b_{\text{NUV}}}$	S_r^*
R1	678	0.264	0.019	0.061
R2	1982	0.280	0.011	0.036
R3	1062	0.279	0.007	0.024
R4	971	0.303	0.016	0.051
R5	1003	0.276	0.023	0.073
R6	443	0.292	0.024	0.078
R7	795	0.263	0.017	0.056
R8	702	0.253	0.020	0.066
R9	671	0.253	0.019	0.062
R10	772	0.261	0.018	0.058

3.2.2 Stellar density as a function of galactic latitude

Stellar density decreases with galactic latitude introducing a bias in the extinction value that has been corrected following GdC2015. A simple inspection of Eq. 2 shows that if N_{NUV}^* depends on galactic latitude, then

$$A_{\text{NUV}} = \frac{1}{b_{\text{NUV}}} \log \left(\frac{N_{\text{NUV}}^{*,b0} N_{\text{NUV}}^{*,b}}{N_{\text{NUV}}^{*,b} N_{\text{NUV}}^*} \right) \quad (3)$$

being the true extinction, A_{NUV}^0 given by,

$$A_{\text{NUV}}^0 = \frac{1}{b_{\text{NUV}}} \log \left(\frac{N_{\text{NUV}}^{*,b}}{N_{\text{NUV}}^*} \right) \quad (4)$$

hence,

$$A_{\text{NUV}}^0 = A_{\text{NUV}} - dA_{\text{NUV}} \quad (5)$$

where dA_{NUV} is the correction factor,

$$dA_{\text{NUV}} = \frac{1}{b_{\text{NUV}}} \log \left(\frac{N_{\text{NUV}}^{*,b0}}{N_{\text{NUV}}^{*,b}} \right) \quad (6)$$

that depends on galactic latitude. To evaluate this correction, we have selected a set of non-extinguished fields and have evaluated dA_{NUV} , using as $N_{\text{NUV}}^{*,b0}$ the maximum value; we have also included a field at $l_{\text{gal}} \sim 208.745$, $b_{\text{gal}} \sim +0.83^\circ$ to reach the Galactic Plane. Then, we have fitted these dA_{NUV} values as a linear function of b_{gal} using the Theil-Sen non-parametric fitting method (see Appendix A for details on the final fit).

3.3 The A_{NUV}/A_K map

Three A_{NUV} maps were computed for pixel sizes 10, 15 and 30 arcmin after applying the method and corrections described above. The infrared data were extracted from F07's map based on 2MASS data.

2MASS performed the most complete near infrared survey of the sky providing JHK magnitudes for 471 million of point sources. There exist numerous dust maps based on 2MASS data (e.g. Lombardi et al. (2011); Juvela & Montillaud (2016)). We have selected the dust map of the Galactic Anticentre by F07 because of its availability

in FITS format as online material that was obtained using the NICE (*Near Infrared Color Excess*) method developed by Lada et al. (1994). As F07 point out, “extinction values in the very dense regions of the clouds in this map are underestimated and there is a small A_V dilution for more distant clouds”. However, as Orion is at a moderate distance (~ 400 pc) and there are not intervening molecular clouds in the line of sight, any geometric effect will affect the same way the extinction measures in NUV and K bands, provided that the pixel size is the same. We could only find underestimated values in the small portion of the filament of Orion A that has been observed by GALEX, which is the densest region in our map.

F07's map was downloaded in FITS format via ftp. We transformed back the F07's A_V map into an A_H map following F07 instructions, and then in an A_K map by applying the interstellar extinction law by FM07: $A_H = 1.666A_K$. The map was then resampled to the selected resolutions (10', 15' and 30') and the ratio A_{NUV}/A_K was computed. The final images are plotted in Fig. 2

In general, at lower latitudes the A_K map contains a large number of negative or zero extinction values due to the scarce sensitivity of near infrared wavelengths to small dust columns, which results in abnormally high A_{NUV}/A_K values. In our maps, the saturation value has been set at 33, which corresponds to the mean value for the ISM (GdC2015). In order to discern the relationship between the high column density areas of gas and the regions of grain growth, we have plotted the relative extinction maps over the dust map by F07.

4 RESULTS: EVIDENCE OF DUST NUCLEATION IN ORION

As Orion is located at $d \sim 400$ pc, the statistics are not good enough for resolving small cores and filaments in the extinction maps; the typical size of cores is 0.1-0.4pc that would correspond to pixel sizes of 0.9-3.4 arcmin. Nevertheless, we can study the large-scale distribution of filaments and condensations.

Low values of A_{NUV}/A_K point out a decrease of the strength of the 2175Å feature and a lack of small dust particles. This could be produced either by dust coagulation as observed in molecular clouds (Flagey et al. (2009)), or by photo evaporation of small dust grains in shocks or heavily irradiated environments.

The resolution of the 30' map is rather rough; however, it is feasible to identify the key areas. Quite low A_{NUV}/A_K values are found around $l_{\text{gal}} \sim 212$, $b_{\text{gal}} \sim -8$. This structure is partially resolved in the 15arcmin map (Fig. 2, middle) where we can distinguish two filaments: the first one parallel to Orion B and the other one intersecting it perpendicularly. Inside the filament we find small cores in the 10arcmin map (Fig. 2, down) with A_{NUV}/A_K values close to zero. Dust nucleation is most likely to be the responsible of this A_{NUV}/A_K drop.

Also, the area within the Orion A filament mapped by GALEX presents small A_{NUV}/A_K values, which is consistent with the high density of gas, favouring the growth of dust grains. In Fig. 3 we compare our A_{NUV}/A_K map around the Orion A molecular cloud with the optical-depth

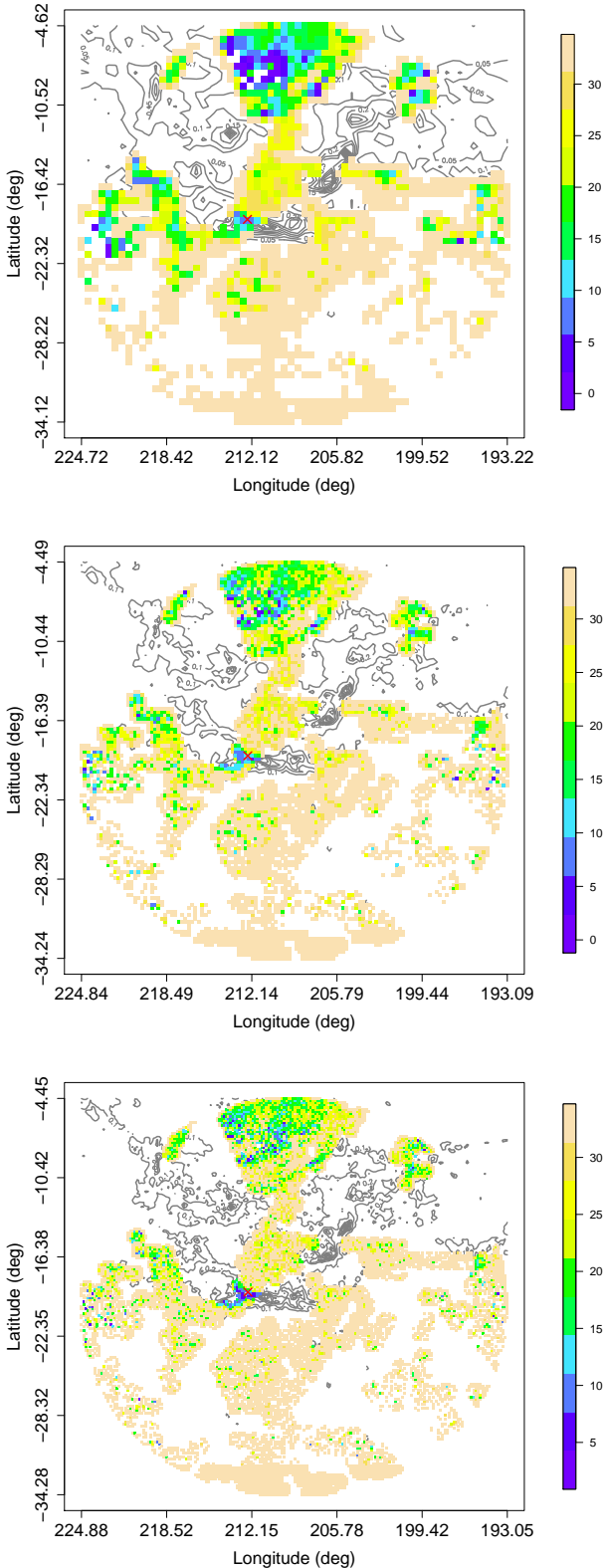


Figure 2. Orion relative extinction maps $A_{\text{NUV}}/A_{\text{K}}$ with pixel sizes of 30arcmin (up), 15arcmin (middle) and 10arcmin (down). Contours correspond to F07’s infrared extinction map. Low $A_{\text{NUV}}/A_{\text{K}}$ values (dark color) indicate a decrease of the strength of the 2175Å bump and a lack of small dust particles. The saturation limit has been set to $A_{\text{NUV}}/A_{\text{K}} = 33$ (light color), the mean value for the ISM (GdC2015). The location of HD 38023, foreground to the cloud, is marked with a cross (see Sec. 5).

temperature map derived by Lombardi et al. (2014) using Herschel, Planck and IRIS data, where color represents the dust effective temperature (red $T \leq 12\text{K}$, blue $T \geq 30\text{K}$) and the optical-depth is proportional to intensity. We can see that there is an overdensity of YSO candidates (S2014) in the portion of the Orion A cloud that has been observed and which corresponds to the densest region (the lowest $A_{\text{NUV}}/A_{\text{K}}$ values). We can also see a filament of moderate $A_{\text{NUV}}/A_{\text{K}}$ values perpendicular to the Orion B cloud, with some slightly dense cores ($A_{\text{NUV}}/A_{\text{K}} \sim 20$) along it. At $l_{\text{gal}} \sim 206^\circ$, $b_{\text{gal}} \sim -19^\circ$ we apparently find another filament with several YSO candidates placed throughout it.

At greater galactic longitudes we find intermediate $A_{\text{NUV}}/A_{\text{K}}$ values coinciding with the edges of the cloud.

In the borders of the λ Orionis bubble ($l_{\text{gal}} \sim 200^\circ$, $b_{\text{gal}} \sim -8^\circ$ and $l_{\text{gal}} \sim 194^\circ$, $b_{\text{gal}} \sim -16^\circ$) there are significant lower values of $A_{\text{NUV}}/A_{\text{K}}$ than in its surroundings. These variations of the strength of the bump could be explained as the result of destruction of PAHs due to the strong UV radiation coming from the massive stellar cluster inside the bubble. The areas mapped by GALEX correspond roughly to clouds L1599 and B223 (see Fig. 4).

Despite the fact that in L1599 our relative extinction values are not remarkably low, they are smaller than those found in the ISM as we are mapping the molecular material that is being swept away inside the bubble. We find a dense core in the outer part of the rim where dust coagulation is presumably taking place.

Computed $A_{\text{NUV}}/A_{\text{K}}$ values match almost perfectly with CO emission from dense, massive dark globules found by Lang et al. (2000) in B223; our statistics predict that intermediate size grains are forming inside these clouds. Moreover, most of YSO candidates selected by S2014 overlap with these cores, which could be an indicative of triggered star formation.

Finally, at $l_{\text{gal}} \sim 221^\circ$, $b_{\text{gal}} \sim -20^\circ$ we find a small isolated but very dense region (Fig. 2, 15 and 10 arcmin), apparently non-extinguished in F07’s map. Nevertheless, after a carefully comparison between GALEX, Herschel and Planck images using ESASky we find tiny molecular cores where Herschel has detected dust grain formation.

5 ROSETTE: TESTING SPECTROSCOPIC VERSUS STATISTICAL METHODS

The Rosette cloud is a well studied structure in the interstellar medium located at $1,330 \pm 48\text{pc}$ from the Sun (Lombardi et al. (2011)). Rosette Nebula is close to the Galactic Plane and it is illuminated by an open cluster of massive stars (NGC 2244, Martins et al. (2012)), which is the main responsible of the cloud ionisation. It is also considered a prototype of triggered star formation and its properties (such as dust temperature and column density) have been recently studied by Schneider et al. (2010) and Schneider et al. (2012) using Herschel data.

We have searched the catalogue of high quality spectra of non-variable sources in the database of the International Ultraviolet Explorer (IUE) (Beitia-Antero & Gómez de Castro (2016)) for UV spectra of massive O-B stars in Orion and Rosette. In Orion we only found a star, HD 38023, foreground to the cloud ($d = 311.8$

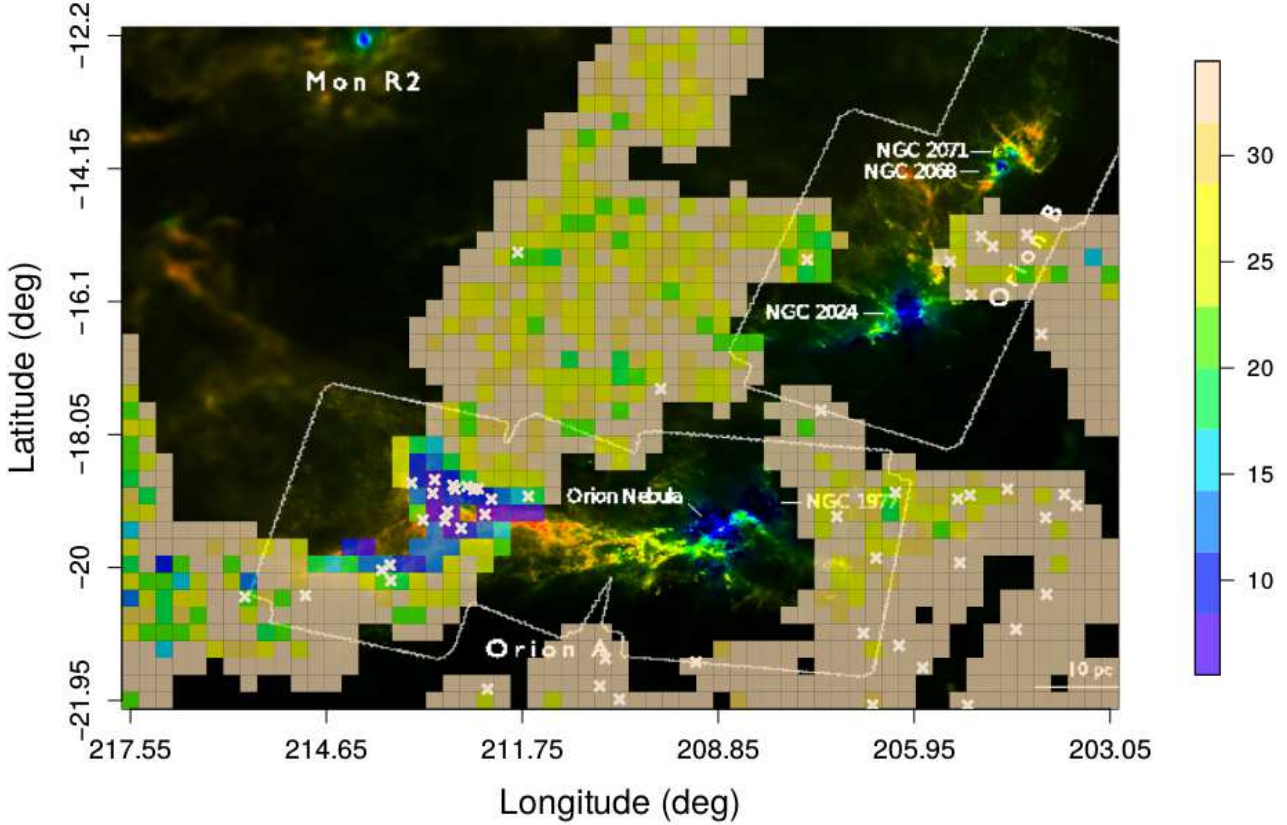


Figure 3. Orion A A_{NUV}/A_K 15arcmin map combined with optical-depth-temperature map by Lombardi et al. (2014). Colors in Lombardi et al. (2014) map represent the dust effective temperature (red $T \leq 12K$, blue $T \geq 30K$) and the optical-depth is proportional to intensity. We can observe a decrease of the UV bump (low A_{NUV}/A_K values) over the Orion A filament, where there exists an overdensity of YSO candidates (white crosses).

pc, see Fig. 2) but due to geometric dilution effects it did not allow us to test our results. However, three O-B stars were found in the IUE catalogue with good spectra in the line of sight to Rosette; two foreground and another roughly the same distance as the cloud (HD 46106, HD 46149 and HD 46056 respectively). The strength of the bump has been assessed from spectroscopic fitting following FM07, $A_{\text{bump}} = \frac{\pi c_3}{2\gamma}$ (see Table 2).

We have also estimated A_{bump} using statistical methods (Eq. 1) since Rosette was mapped during the last period of GALEX’s life (DR6/7, Bianchi et al. (2014)): a grand total of 22 tiles covering $\sim 78\text{deg}^2$ and containing 52,833 point-like NUV sources in a search radius of 2° . As for Orion, a cross-correlation test with the 2MASS catalogue has been run to ascertain that all of them are bona-fidae astronomical sources; only 17,384 sources had a 2MASS counterpart. The NUV luminosity function was found to be the same that in Orion and the galactic latitude correction was applied as in Orion. F07’s map has been used to compute the A_{NUV}/A_K maps for pixel sizes of 10 and 15 arcmin shown in Fig. 5. The image shows the well know Rosette core and filaments.

Both HD 46106 and HD 46149 are foreground to the cloud and have a prominent bump that agrees with the

Table 2. FM07’s c_3 and γ coefficients, spectroscopic and statistical A_{bump} values for OB stars in Rosette.

Star	HD 46106	HD 46149	HD 46056
d (pc)	809.6	1123.1	1343.9
l_{gal}	206:11:55	206:13:12	206:20:09
b_{gal}	-02:05:38	-02:02:20	-02:14:50
c_3	2.93 ± 0.10	3.25 ± 0.14	2.87 ± 0.12
γ	0.86 ± 0.01	0.90 ± 0.02	0.88 ± 0.01
Spectroscopic A_{bump}	5.35 ± 0.24	5.67 ± 0.37	5.12 ± 0.27
$(\frac{A_{\text{NUV}}}{A_K})_{\text{map}}$	20	20	12
Statistical A_{bump}	4.1 ± 0.3	4.1 ± 0.3	3.3 ± 0.3

expectations of the ISM model (FM07); notice that the strength increases with distance, *i. e.*, with dust column. In the same line of sight, but the same distance as Rosette, both spectroscopic (HD 46056) and statistical methods provide the lowest value, suggesting the destruction of small dust grains in the proximity of the cloud (either through coagulation to larger structures or by photodestruction).

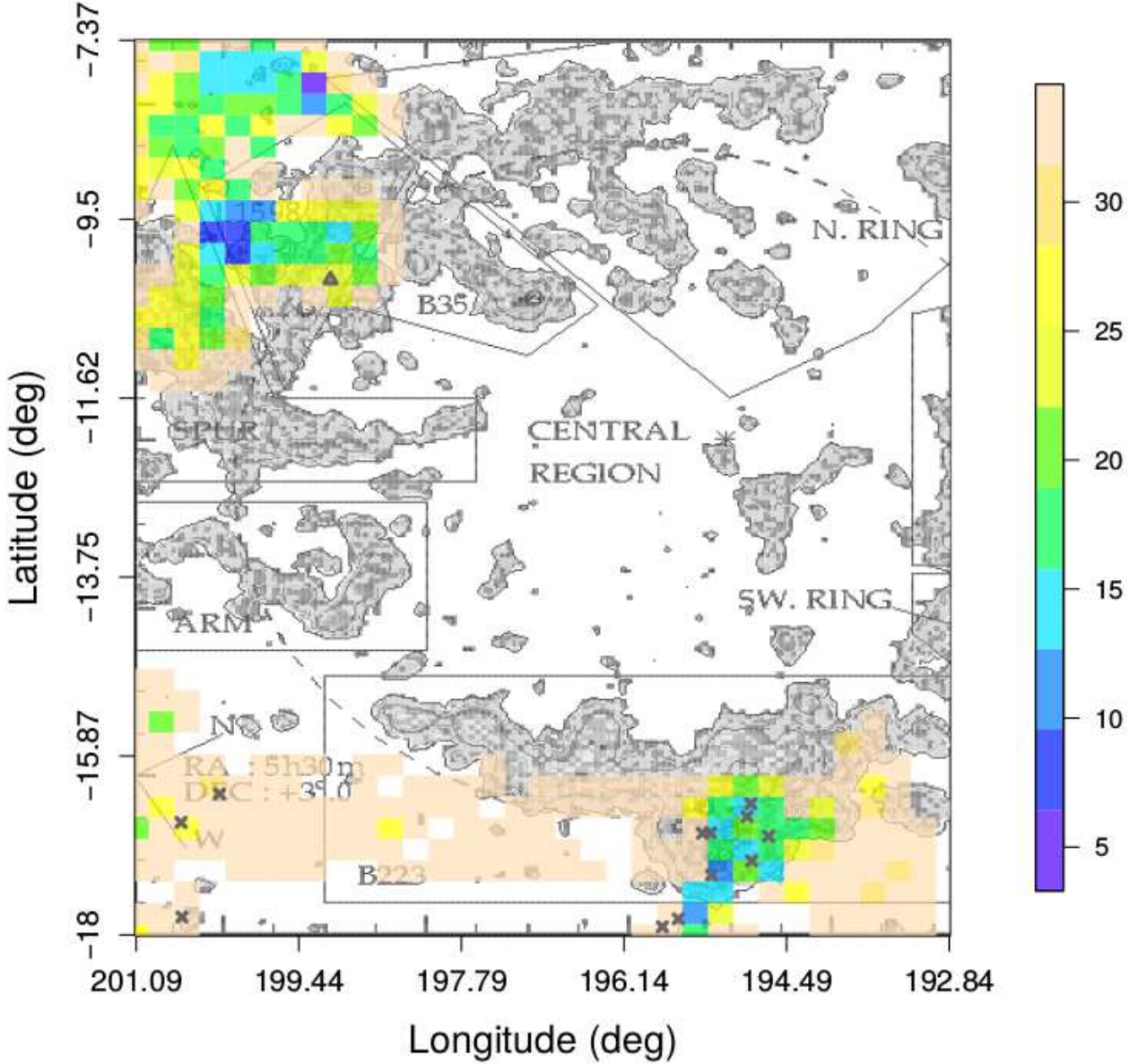


Figure 4. λ Orionis $A_{\text{NUV}}/A_{\text{K}}$ 15 arcmin map combined with CO map by Lang et al. (2000). In the area observed by GALEX we find smaller $A_{\text{NUV}}/A_{\text{K}}$ values than in the ISM; this fact could be explained as a destruction of PAHs or dust grains due to the UV radiation coming from the stellar cluster. Areas of special interest are B223 at the bottom of the image, where there is a gathering of YSO (crosses) and L1599 cloud, marked with a triangle. A small, dense core is found in the outer part of the rim, near L1599 cloud.

To summarise, spectroscopic values are consistently higher than those derived from statistical averages obtained over large physical regions; the typical size of an ISM cloud is about 2-5 pc and our 10 arcmin pixel corresponds to 3.87 pc at Rosette’s distance.

6 CONCLUSIONS

In this work we have applied the method developed by GdC2015 to study the distribution and properties of dust in the ISM and molecular clouds through UV and near infrared relative extinction maps. The main conclusions that we derive are:

- There are not significant variations in the NUV luminosity function in the Galactic Anticentre, and we have ob-

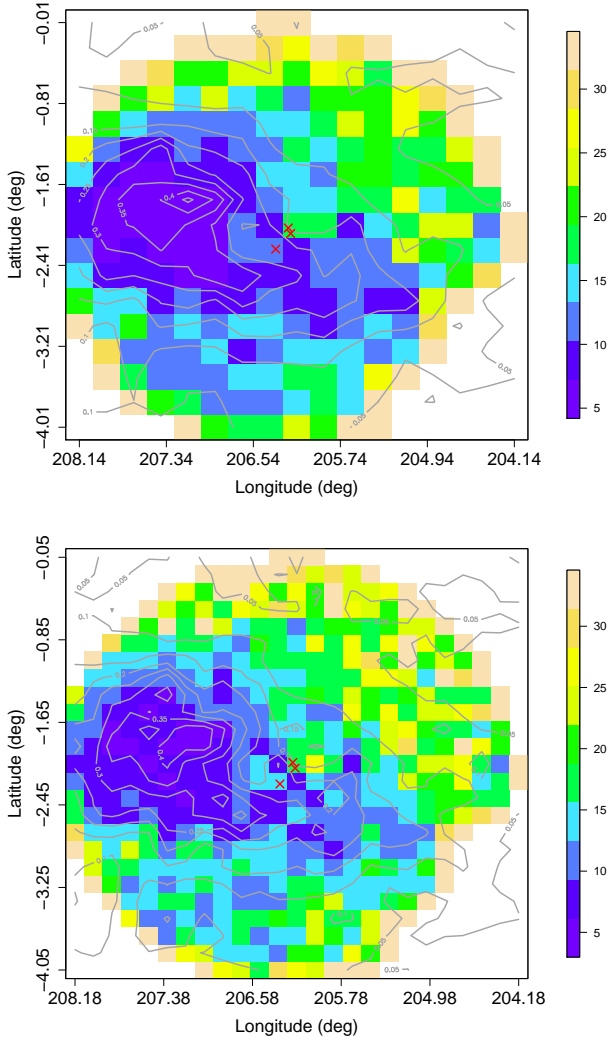


Figure 5. Rosette relative extinction map $A_{\text{NUV}}/A_{\text{K}}$ with pixel sizes of 15arcmin (up) and 10arcmin (down). Contours correspond to F07’s infrared extinction map; the colour coding is the same as in Fig 2. Low $A_{\text{NUV}}/A_{\text{K}}$ values are detected in the Rosette core. IUE stars HD 46023, HD 46106 and HD 46149 are marked with a cross. Statistical A_{bump} values for these stars, using Eq. 1, are 4.1 ± 0.3 , 4.1 ± 0.1 and 3.3 ± 0.3 respectively, while FM07’s spectroscopic values ($A_{\text{bump}} = \frac{\pi c^3}{27}$) are 5.35 ± 0.24 , 5.67 ± 0.37 and 5.12 ± 0.27 .

tained an average value consistent with the value derived by GdC2015 in Taurus.

- Variations of the strength of the 2175 Å bump in relative extinction maps reveal the growth of dust grains in some dense areas, like Orion A, as well as a possible destruction of PAHs in the λ Orionis molecular ring.

- Spectroscopic data provide $A_{\text{NUV}}/A_{\text{K}}$ values slightly higher than those obtained by statistical methods because of the large pixel sizes.

- The extinction values obtained by this method are statistically averaged, so they are fairly reliable when the molecular clouds are at a moderate distance like Orion but they are diluted at larger distances (as in Rosette).

ACKNOWLEDGEMENTS

We would like to thank the referee for his/her comments that substantially improved our manuscript. This work has been funded by the Ministry of Economy and Competitiveness of Spain through grants: ESP2014-54243-R and ESP2015-68908-R. Leire Beitia-Antero acknowledges the receipt of a “Beca de Excelencia” from the Universidad Complutense de Madrid.

This work has made use of data from the European Space Agency (ESA) mission *Gaia* (<http://www.cosmos.esa.int/gaia>), processed by the *Gaia* Data Processing and Analysis Consortium (DPAC, <http://www.cosmos.esa.int/web/gaia/dpac/consortium>). Funding for the DPAC has been provided by national institutions, in particular the institutions participating in the *Gaia* Multilateral Agreement.

REFERENCES

- Beitia-Antero L., Gómez de Castro A. I., 2016, *A&A*, 596, A49
 Bianchi L., Efremova B., Herald J., et al., 2011, *MNRAS*, 411, 2770
 Bianchi L., Herald J., Efremova B., et al., 2012, *VizieR Online Data Catalog*, 2312
 Bianchi L., Conti A., Shiao B., 2014, *VizieR Online Data Catalog*, 2335
 Bok B., Cordwell C., 1973, in Gordon M., Snyder L., eds, *Molecules in the Galactic Environment*. p. 54
 Draine B., 2003, *ARA&A*, 41, 241
 Dzyurkevich N., Benoît C., Lesaffre P., et al., 2017, arXiv:1702.05688v1
 Elmegreen B., 1990, *ApJ*, 357, 125
 Fitzpatrick E., Massa D., 2007, *ApJ*, 663, 320
 Flagey N., et al., 2009, *ApJ*, 701, 1450
 Franco J., et al., 2002, *ApJ*, 570, 647
 Froebrich D., Murphy G., Smith M., et al., 2007, *MNRAS*, 378, 1447
 Gaia Collaboration et al., 2016, *A&A*, 595, A2
 Gómez de Castro A. I., Lopez-Santiago J., Sestito P., et al., 2011, *Ap&SS*, 335, 97
 Gómez de Castro A. I., López-Santiago J., López-Martínez F., et al., 2015, *MNRAS*, 449, 3867
 Juvela M., Montillaud J., 2016, *A&A*, 585, A38
 Lada C., Lada E., Clemens D., et al., 1994, *ApJ*, 429, 694
 Lang W., Masheder M., Dame T., et al., 2000, *A&A*, 357, 1001
 Leger A., Puget J., 1984, *A&A*, 137, L5
 Lombardi M., Alves J., Lada C., 2011, *A&A*, 535
 Lombardi M., Bouy H., Alves J., et al., 2014, *A&A*, 566, A45
 Martin D., Fanson J., Schiminovich D., et al., 2005, *ApJ*, 619, L1
 Martins F., Mahy L., Hillier D., et al., 2012, *A&A*, 538, A39
 Mirabel I., 1982, *ApJ*, 256, 120
 Nakano T., 1998, *ApJ*, 494, 587
 Pilipp W., Hartquist T., Havnes O., Morfill G., 1987, *ApJ*, 314, 341
 Roy A., Martin P., Polychroni D., et al., 2013, *ApJ*, 763, 55
 Sánchez N., Gómez de Castro A. I., López-Martínez F., et al., 2014, *A&A*, 572
 Schneider N., Motte F., Bontemps S., et al., 2010, *A&A*, 518, L83
 Schneider N., Csengeri T., Hennemann M., et al., 2012, *A&A*, 540, L11
 Skrutskie M., Cutri R., Stiening R., et al., 2006, *AJ*, 131, 1163
 Stutz A., Kainulainen J., 2015, *A&A*, 577, L6
 Wang J., et al., 2004, *ApJ*, 614, L105
 Weingartner J., Draine B., 2001, *ApJ*, 553, 581
 Ysard N., Abergel A., Ristorcelli I., et al., 2013, *A&A*, 559, A133

Table A1. Theil-Sen linear fitting results for the galactic latitude correction term. m denotes the slope, while n is the intercept.

Map	m	err_m	n	err_n	S_r
30arcmin	-0.075	0.045	-0.307	0.192	0.218
15arcmin	-0.082	0.056	-0.421	0.223	0.250
10arcmin	-0.073	0.042	-0.401	0.192	0.220

APPENDIX A: GALACTIC LATITUDE CORRECTION

The correction factor has been evaluated for all pixel sizes, 10, 15 and 30 arcmin. In the process, evidence was found of a real variation of the data with galactic latitude (but not with longitude) and thus a parametric fit could not be performed.

Hence, dA_{NUV} values were fit as a linear function of b_{gal} , $dA_{\text{NUV}} = m + n \times b_{\text{gal}}$, using the Theil-Sen method (see Figure A1). dA_{NUV} , m and n , together with residual standard error (S_r) of the fittings are given in Table A1 for the three pixel sizes considered. $N_{\text{NUV}}^{*,b0}$ was measured in the $l_{\text{gal}} \sim 214^\circ.745$, $b_{\text{gal}} \sim -8^\circ$, field.

This paper has been typeset from a $\text{\TeX}/\text{\LaTeX}$ file prepared by the author.

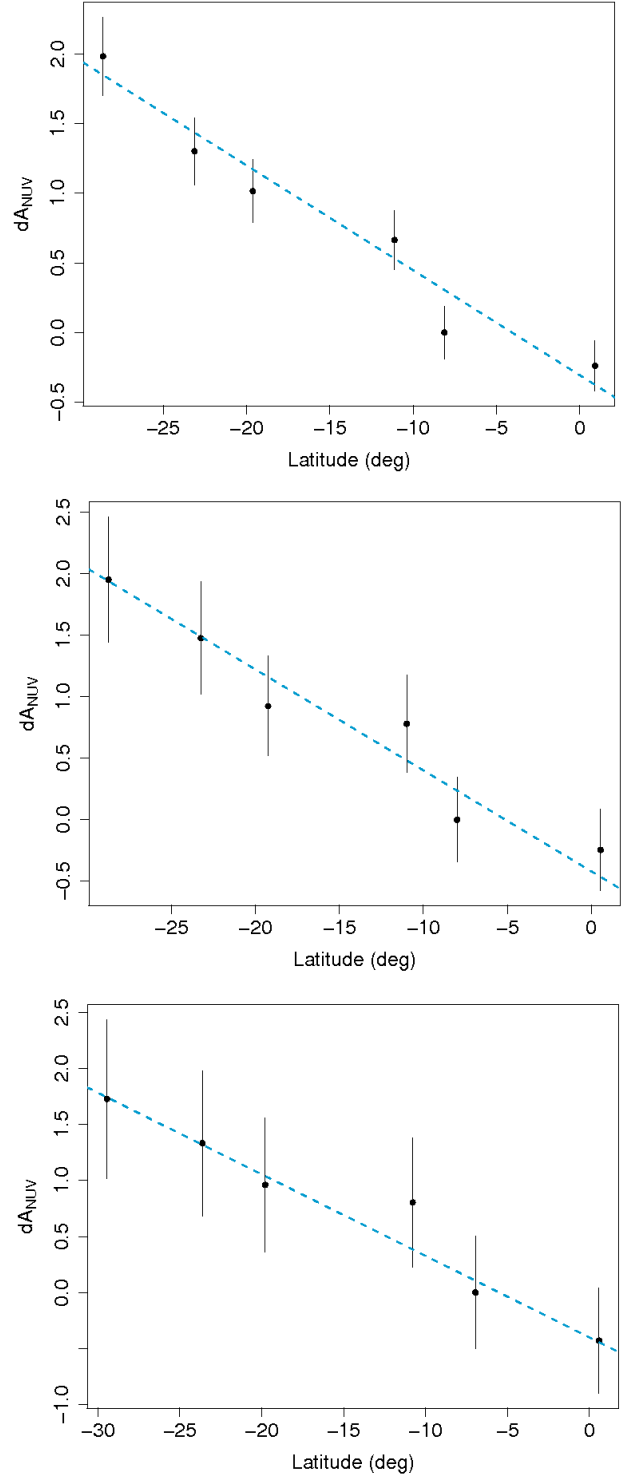


Figure A1. Theil-Sen linear fitting curves (top: 30arcmin; middle: 15arcmin; bottom: 10arcmin) for the galactic latitude correction term dA_{NUV} . In all cases, the reference value was considered to be at $l_{\text{gal}} \sim 214^\circ.745$, $b_{\text{gal}} \sim -8^\circ$. The dashed line corresponds to the linear fitting.